This Accepted Manuscript has not been copyedited and formatted. The final version may differ from this version. A link to any extended data will be provided when the final version is posted online.

JNeurosci
THE JOURNAL OF NEUROSCIENCE

Research Articles: Neurobiology of Disease

Increased lysosomal exocytosis induced by lysosomal Ca^{2+} channel agonists protects human dopaminergic neurons from α-synuclein toxicity

Taiji Tsunemi[1,3], Tamara Perez-Rosello[2], Yuta Ishiguro[3], Asako Yoroisaka[3], Sohee Jeon[1], Kana Hamada[1], Malini Krishna Vangipuram Suresh[1], Yvette C. Wong[1], Zhong Xie[2], Wado Akamatsu[4], Joseph R. Mazzulli[1], D. James Surmeier[2], Nobutaka Hattori[3] and Dimitri Krainc[1]

[1]Ken & Ruth Davee Department of Neurology, Northwestern University Feinberg School of Medicine, 303 East Chicago Avenue, Ward 12-226, Chicago, Illinois 60611, USA.

[2]Department of Physiology, Northwestern University Feinberg School of Medicine, 310 East Superior Street, Morton 5-660, Chicago, Illinois 60611, USA.

[3]Department of Neurology, Juntendo University School of Medicine, 2-1-1, Hongo, Bunkyo-ku, Tokyo 113-8421, Japan.

[4]Center for Genomic and Regenerative Medicine, Juntendo University School of Medicine, 2-1-1, Hongo, Bunkyo-ku, Tokyo 113-8421, Japan.

https://doi.org/10.1523/JNEUROSCI.3085-18.2019

Received: 8 December 2018

Revised: 6 April 2019

Accepted: 4 May 2019

Published: 16 May 2019

Author contributions: T.T. and D.K. designed research; T.T., T.P.-r., Y.I., A.Y., S.J., K.H., M.K.V.S., and Z.X. performed research; T.T. and J.R.M. analyzed data; T.T. wrote the first draft of the paper; T.T. and D.K. wrote the paper; Y.C.W., W.A., J.R.M., D.J.S., N.H., and D.K. edited the paper.

Conflict of Interest: The authors declare no competing financial interests.

This work is supported by National Institute of Health (R37 NS096241) to DK and JSPS KAKENHI Grants (16H07185) and (18K07510); Brains research foundation; Juntendo University Research Institute for Diseases of Old Age and Environmental & Gender-specific Medicine to T.T.

Correspondence should be addressed to To whom correspondence should be addressed: Dr. Dimitri Krainc, Department of Neurology, Northwestern University Feinberg School of Medicine, 303 East Chicago Avenue, Ward 12-140 (office), 312-503-3936 (phone), 312-503-3951 (fax), Email: dkrainc@nm.org

Cite as: J. Neurosci 2019; 10.1523/JNEUROSCI.3085-18.2019

Alerts: Sign up at www.jneurosci.org/alerts to receive customized email alerts when the fully formatted version of this article is published.

Accepted manuscripts are peer-reviewed but have not been through the copyediting, formatting, or proofreading process.

Copyright © 2019 the authors

JNeurosci Accepted Manuscript

JNeurosci Accepted Manuscript

1 **Title: Increased lysosomal exocytosis induced by lysosomal Ca^{2+} channel agonists protects**
2 **human dopaminergic neurons from α-synuclein toxicity**
3
4

5 **Authors:** Taiji Tsunemi[1,3], Tamara Perez-Rosello[2], Yuta Ishiguro[3], Asako Yoroisaka[3], Sohee
6 Jeon[1], Kana Hamada[1], Malini Krishna Vangipuram Suresh[1], Yvette C. Wong[1], Zhong Xie[2], Wado
7 Akamatsu[4], Joseph R. Mazzulli[1], D. James Surmeier[2], Nobutaka Hattori[3], Dimitri Krainc[1*]
8
9 **Affiliations:**
10 1. Ken & Ruth Davee Department of Neurology, Northwestern University Feinberg School of
11 Medicine, 303 East Chicago Avenue, Ward 12-226, Chicago, Illinois 60611, USA.
12
13 2. Department of Physiology, Northwestern University Feinberg School of Medicine, 310 East
14 Superior Street, Morton 5-660, Chicago, Illinois 60611, USA.
15
16 3. Department of Neurology, Juntendo University School of Medicine, 2-1-1, Hongo, Bunkyo-
17 ku, Tokyo 113-8421, Japan.
18
19 4. Center for Genomic and Regenerative Medicine, Juntendo University School of Medicine, 2-
20 1-1, Hongo, Bunkyo-ku, Tokyo 113-8421, Japan.
21
22 *To whom correspondence should be addressed:
23 Dr. Dimitri Krainc
24 Department of Neurology
25 Northwestern University Feinberg School of Medicine
26 303 East Chicago Avenue
27 Ward 12-140 (office)
28 312-503-3936 (phone)
29 312-503-3951 (fax)
30 Email: dkrainc@nm.org
31
32

33 **Key Words:** lysosomal exocytosis, Parkinson's disease (PD), Kufor-Rakeb syndrome (KRS),
34 PARK9/ATP13A2, alpha synuclein, induced pluripotent stem cells (iPSCs), dopaminergic
35 neurons, TRPML1, lysosomal Ca^{2+} channel
36

37 **Abstract**: The accumulation of misfolded proteins is a common pathological feature of many
38 neurodegenerative disorders, including synucleinopathies such as Parkinson's disease which is
39 characterized by the presence of α-synuclein (α-syn) containing Lewy bodies. However, while
40 recent studies have investigated α-syn accumulation and propagation in neurons, the molecular
41 mechanisms underlying α-syn transmission have been largely unexplored. Here, we examined

JNeurosci Accepted Manuscript

a monogenic form of synucleinopathy caused by loss of function mutations in lysosomal ATP13A2/PARK9. These studies revealed that lysosomal exocytosis regulates intracellular levels of α-syn in human neurons. Loss of PARK9 function in patient-derived dopaminergic neurons disrupted lysosomal Ca^{2+} homeostasis, reduced lysosomal Ca^{2+} storage, increased cytosolic Ca^{2+} and impaired lysosomal exocytosis. Importantly, this dysfunction in lysosomal exocytosis impaired α-syn secretion from both axons and soma, promoting α-syn accumulation. However, activation of the lysosomal Ca^{2+} channel – transient receptor potential mucolipin 1 (TRPML1) – was sufficient to upregulate lysosomal exocytosis, rescue defective α-syn secretion and prevent α-syn accumulation. Together, these results suggest that intracellular α-syn levels are regulated by lysosomal exocytosis in human dopaminergic neurons, and may represent a potential therapeutic target for Parkinson's disease and other synucleinopathies.
(182 words)

Significant Statement: Parkinson's disease is the second most common neurodegenerative disease linked to the accumulation of a-synuclein in patient neurons. But it is unclear what this mechanism might be. Here, we demonstrate a novel role for lysosomal exocytosis in clearing intracellular a-synuclein, and show that impairment of this pathway by mutations in the Parkinson's disease-linked gene ATP13A2/PARK9 contributes to a-synuclein accumulation in human dopaminergic neurons. Importantly, upregulating lysosomal exocytosis by increasing lysosomal Ca^{2+} levels is sufficient to rescue defective a-synuclein secretion and accumulation in patient neurons. These studies identify lysosomal exocytosis as a potential therapeutic target in diseases characterized by the accumulation of a-synuclein including Parkinson's disease.
(96 words)

JNeurosci Accepted Manuscript

67 **Main Text:**

68 **Introduction**

69 Parkinson's disease (PD) is pathologically characterized by the deposition of Lewy bodies and
70 neurites composed of alpha-synuclein (α-syn), a presynaptic protein implicated in the
71 pathogenesis of sporadic and familial PD (Wong and Krainc, 2017). Increased α-syn expression
72 is toxic to neurons, as duplication of the α-syn *SNCA* locus causes late-onset PD, while
73 triplication leads to early-onset PD suggesting that α-syn-mediated neurotoxicity is dose-
74 dependent (Chartier-Harlin et al., 2004, Ibanez et al., 2004, Singleton et al., 2003). Recent
75 genetic studies have also implicated lysosomal dysfunction as a key player in PD pathogenesis,
76 as several genes encoding lysosomal proteins have been linked to familial forms of PD (Mc
77 Donald and Krainc, 2017), including *ATP13A2/PARK9* whose loss of function mutations result in
78 Kufor-Rakeb syndrome (KRS), a rare hereditary neurodegenerative disorder (Ramirez et al.,
79 2006).
80
81 *PARK9* encodes a lysosomal Type 5 P-type ATPase involved in cation homeostasis (Gitler et al.,
82 2009, Kong et al., 2014, Park et al., 2014, Tsunemi et al., 2014), whose loss of function leads to
83 lysosomal dysfunction (Bento et al., 2016, Dehay et al., 2012, Lopes da Fonseca et al., 2016,
84 Usenovic et al., 2012). ATP13A2/PARK9 also localizes to multivesicular bodies and contributes
85 to the formation of intraluminal vesicles (ILVs), and may regulate sorting and trafficking of
86 cargos through inositol phosphate(3,5)P2 binding to the N-terminus of PARK9 (Demirsoy et al.,
87 2017, Holemans et al., 2015). Loss of PARK9 function in patient fibroblasts leads to α-syn
88 accumulation (Tsunemi, et al., 2014), but whether α-syn also accumulates in patient
89 dopaminergic neurons and whether the molecular machinery contributing to α-syn
90 accumulation is amenable to therapeutic interventions remain unknown. Importantly,
91 identifying the cellular pathways and targets which regulate intracellular α-syn levels in human
92 neurons will provide relevant therapeutic strategies for combatting α-syn-mediated
93 neurotoxicity in multiple forms of synucleinopathies.
94
95 Using iPSC-derived dopaminergic neurons from KRS (PARK9) patients expressing mutant *PARK9*,
96 we found that PARK9 plays a critical role in regulating lysosomal exocytosis. Patient neurons
97 exhibit decreased secretion of α-syn from both the axon and the cell body, as well as disrupted
98 lysosomal Ca^{2+} homeostasis, leading to defective lysosomal exocytosis. Surprisingly, enhancing
99 lysosomal exocytosis using drugs targeting the lysosomal Ca^{2+} channel TRPML1 increased
100 lysosomal exocytosis and α-syn secretion, and attenuated α-syn intracellular accumulation in
101 patient neurons. Thus, upregulation of neuronal secretion may be a potential key target for
102 developing viable therapies for KRS and other related synucleinopathies such as PD.
103 (331 words)
104

105 **Materials and Methods**

106 ***Cell culture***

107 Human neuroglioma cell line (H4)-expressing wild-type α-syn under the control of a tetracycline
108 inducible promoter and primary dermal fibroblasts taken from four normal and two *PARK9*
109 patients (1550 C>T; MUT1 and 3176 T>G, 3253 delC; MUT2) were cultured as described

JNeurosci Accepted Manuscript

110 previously (Dehay, et al., 2012, Grunewald et al., 2012, Mazzulli et al., 2016b, Tsunemi and
111 Krainc, 2014, Tsunemi, et al., 2014, Usenovic, et al., 2012). Mut1 carries homozygous missense
112 mutations in *ATP13A2* alleles (c. 1550C>T/c. 1550C>T) that result in homozygous amino acid
113 substitutions in ATP13A2 proteins (p.T517I/p.T517I). Mut2 carries compound heterozygous
114 mutations: one is a missense mutation that results in an amino acid substitution (c. 3176 T>G, p
115 p.L1059R) and the other is a single nucleotide deletion (3253 delC) that results in many amino
116 acid alternations with an appearance of a premature stop codon. All human induced
117 pluripotent stem (iPS) cells were reprogrammed as described previously (Mazzulli et al., 2016a).
118 Briefly, the four distinct factors (OCT4, SOX2, cMYC and KLF4) were transfected into human skin
119 fibroblasts using retroviral system. Three control (Cont 1, Cont 2 and Cont 3) and one mutant
120 (Mut 2) iPSCs were characterized previously (Cooper et al., 2012, Mazzulli, et al., 2016b). One
121 control (Cont 4) and one mutant (Mut 1) iPSCs were characterized for spontaneous
122 differentiation analysis and the expression of pluripotency markers (Fig. 1-1). All iPSCs were
123 cultured on irradiated mouse embryonic fibroblasts (MEF) in iPS cell media containing
124 DMEM/F12 (Stem Cell Technologies) with 20% knock-out serum replacement (Invitrogen), L-
125 glutamine, nonessential amino acids, 2-mercaptoethanol (Invitrogen), 10 ng/ml FGF-Basic (AA1-
126 155) recombinant human protein (Invitrogen), and penicillin/streptomycin at 37°C in 5% CO_2.
127 Differentiation towards dopaminergic neurons was conducted following the protocol described
128 previously (Mazzulli, et al., 2016a). At 40 days after the initiation of differentiation, we infected
129 lentiviruses depending on the experiments. Immunocytochemical analysis revealed
130 neuralization efficiency in DA neurons using neuron specific, β-iii-tubulin and midbrain specific
131 markers (TH, FOXA2 and LMX1a). The proportion of neurons coexpressing TH and FOXA2 from
132 day 40 and at day 120 was similar among all the cell lines (Fig. 1-2).
133
134 ***Immunocytochemistry***
135 Immunocytochemical analysis was conducted as described previously (Tsunemi and Krainc,
136 2014, Tsunemi, et al., 2014). Briefly, after fixation in 4% paraformaldehyde, the cells were
137 permeabilized/blocked in PBS containing 0.1% saponin, 1% BSA and 5% normal goat serum for
138 20 min. Specimens were then incubated with primary antibodies overnight, washed in PBS, and
139 then incubated with Alexa conjugated anti-rabbit or anti-mouse antibodies at 1:400 dilution for
140 one hour. Confocal imaging was conducted on the Leica TCS SPE confocal system with Leica
141 DMI 4000B CSQ inverted microscope equipped with an ACS APO 63× (1.3 numerical aperture)
142 oil-immersion objective. For quantification analysis, 10,000 cells/well were plated in triplication
143 and fluorescence intensity was measured using SpectraMax i3 multimode microplate reader
144 (Molecular Devices). Epifluorescence imaging was performed on a Leica DMI3000 B inverted
145 microscope. Live cell imaging was conducted on the Zeiss LSM 780 confocal microscope system
146 with the Zeiss AxioObserver. Z1 inverted microscope equipped with an alpha Plan-Apochromat
147 100X/1,46 Oil DIC M27 objective. Cells were maintained at 37 C° and 5% CO_2 on the
148 temperature controlled heating stage in a CO_2 controlled incubator.
149
150 ***Electrophysiological recordings***
151 Spontaneous pacemaking activity was recorded on iPSC-derived DA neurons from healthy
152 controls and *PARK9*-mutant KRS patients (78-85 post-differentiation). Cultures were transferred
153 to a recording chamber on a fixed-stage inverted microscope (Diaphot 200; Nikon). Interleaved

JNeurosci Accepted Manuscript

recordings from controls and *PARK9* patients were performed at 32°C. The recording chamber was perfused (1-2 ml/min) with Hepes-based solution (in mM): 140 NaCl, 5 KCl, 1 $MgCl_2$, 2 $CaCl_2$, 10 Hepes, 10 glucose, 10 sucrose; pH 7.4, osmolarity 300-305 mOsm/L. Blockers of excitatory and inhibitory transmission were included. Patch pipettes (3–5 MΩ) were filled with internal solution containing the following (in mM): 135 K-$MeSO_4$, 5 KCl, 5 HEPES, 0.05 EGTA, 10 phosphocreatine-di(tris), 2 ATP-Mg, 0.5 GTP- Na, pH: 7.25– 7.30, osmolarity: 285–295 mOsm/L. Recording patch pipettes were prepared with a horizontal puller (model P-97; Sutter Instruments) using borosilicate glass with filament (outer diameter 1.5 mm, inner diameter 0.86 mm). Somatic cell-attached voltage-clamp recordings were obtained with a Multi-Clamp 700B amplifier (Molecular Devices) interfaced to a Pentium-based PC running pClamp 10.6 (Molecular Devices). The signals were filtered at 1 kHz and digitized at 10 kHz with a Digidata 1440A (Molecular Devices). Analysis of instantaneous firing frequency were done in Clampfit 10.6 (Molecular Devices).

Ca^{2+} imaging

Ca^{2+} imaging was conducted as described previously (Dryanovski et al., 2013). After stained with 1 µM Fura2-AM solution for 30 minutes, neurons on coverslips were washed once, and placed on the imaging chamber mounted on the inverted epifluorescence microscope (IX71; Olympus) with xenon illumination. Neurons were imaged using a CCD camera (I-PentaxMax: Princeton Instruments) operated by a Pentium-based PC running MetaFluor imaging software (Molecular Devices). The imaging chamber was superfused with HEPES-buffered ACSF as the flow rate of 2-3 ml/min. Experiments were conducted at room temperature with a 40×/1.35 NA oil-immersion objective (Olympus). Regions of interests (ROIs) were chosen in the soma and at various distances. The two excitation filters (340 and 380 nm) were mounted on a Lambda 10–2 filter wheel (Sutter Instruments), which allowed for rapid and accurate switch between the two wavelengths. The emission was monitored at 520 nm. Ratiometric images (F_{340}/F_{380}) were taken every 3 s with exposure time of 200 ms. For measuring lysosomal Ca^{2+} concentration, Rhod dextran, Potassium Salt, 10,000 MW, Anionic (High-Affinity Version) and Dextran, Cascade blue®, 10,000 MW were used at the concentrations of 0.25 µg/µl and 0.1 µg/µl, respectively. Cells were incubated for 1 hour at 37 °C before washing with Ringer's solution (116 mM NaCl, 2.9 mM KCl, 1.8 mM $CaCl_2$, 5.6 mM HEPES pH 7.2).

Cell-surface staining and biotinylation assay

Cell-surface staining was conducted as described previously (Samie et al., 2013). Briefly, after *PARK9* expression levels were modulated, H4 cells were treated with 200 nM Baf1 for 2 hours and incubated with the LAMP 1 luminal domain antibody (AF 4800, R&D systems) for 1 hour on ice. Cell-surface biotinylated proteins were collected as described previously (Tarradas et al., 2013). After *PARK9* levels were modulated by transfecting *PARK9* shRNA, Scrb shRNA, plasmids containing *PARK9* cDNA or empty vectors for 24 hours, H4 cells cultured in 6-well dishes were treated with 200 nM Baf1 for the indicated period of time. After washing with ice-cold PBS, cells were incubated in PBS with 300 µM EZ-Link™ Sulfo-NHS-SS-Biotin (Thermo Scientific) for 30 min at 4 °C. After biotinylated proteins were lysed in RIPA buffer, 10% of cell lysates were put aside for the INPUT samples and the remaining lysates were incubated with NeutrAvidin™ Agarose

JNeurosci Accepted Manuscript

197 (Thermo Scientific) for 1 hour. The agarose beads were washed with PBS and bound proteins
198 were eluted by heating in gel loading buffer. LAMP-1 levels were analyzed by immunoblotting.
199
200 ***Exosome isolation and nanoparticle tracking analysis***
201 Exosomes were purified as described previously (Tsunemi, et al., 2014). Briefly, exosomes were
202 collected from cell-conditioned media using a basic differential centrifugation method (200 × *g*
203 for 5 min, 1200 × *g* for 10 min, and 16,500 × *g* for 30 min), followed by ultracentrifugation at
204 110,000 × *g* for 60 min. After washing in PBS, exosomes were collected by a centrifugation at
205 110,000 × *g* for 60 min. Analysis of extracellular vesicles was conducted by NanoSight LM10
206 system (NanoSight), configured with a 405 nm laser and a high-sensitivity digital camera system
207 (OrcaFlash2.8, Hamamatsu C11440, NanoSight). Samples were administered and recorded for 1
208 min under sustained flow controlled by script control system equipped with the NanoSight
209 syringe pump. Videos were analyzed by the NTA-software (v2.3).
210
211 ***Lysosomal proteolysis in live neurons and lysosomal enzyme activity assays***
212 Long-lived protein degradation assays were performed by radioactive pulse-chase using tritium-
213 labeled leucine (Perkin-Elmer, #NET460A001MC) as previously described (Kaushik and Cuervo,
214 2009). Enzyme activity assays were performed using the artificial enzyme substrates 4MU-
215 glucopyranoside (for GCase) and 4MU-sulfate potassium salt (for a-i-2-sulf) as described
216 previously. The β-glucocerebrosidase activities were measured as described previously
217 (Mazzulli et al., 2011). The activities of β-hexosaminidase and acid phosphatase were measured
218 following the manufacture's protocols (Sigma).
219
220 ***Alpha synuclein detection***
221 Alpha synuclein ELISA was conducted as described previously (Tsunemi, et al., 2014). Alpha
222 synuclein oligomers/fibrils were formed as described previously (Mazzulli, et al., 2011). Briefly,
223 after α-syn monomers were incubated at 37°C for 10 days under continuous agitation of 1000
224 rpm, α-syn oligomers/fibrils were centrifuged at 10,000 x *g* for 30 min. The pellets were re-
225 suspended in PBS and fibril formation was assessed by Thioflavin T spectroscopic assay and
226 electron microscopic analysis. Alexa Fluor® succinimidyl esters (NHS esters) 555 was conjugated
227 to sonicated α-syn oligomers/fibrils following the manufacturer's instruction (Thermo Fisher
228 Scientific). Briefly, 20 µl of 1 M sodium bicarbonate was added to 200 µl of α-syn
229 oligomers/fibrils (1 mg/ml). Alexa Fluor® was mixed to the solution as the degree of labeling
230 (Bliederhaeuser et al.) became three. The reaction mixture was continued at room
231 temperature for 15 min and stopped by adding 22 µl of 1 M Tris pH 7.4 to the solution.
232 Purification of the proteins from unconjugated dye was performed by Slide-A-Lyzer™ Dialysis
233 Cassettes (2 K WMCO, 0.5 ml, Thermo Fisher Scientific). Alexa Fluor® 555 conjugation was
234 confirmed by Mass spectrometry. For α-syn-Alexa 555 axonal transport assay, DA neurons were
235 plated on the left chambers in microfluidic devices at day 24 from the start of differentiation
236 (SND450, Xona Microfluidics, LLC, Temecula, CA). At day 60, α-syn-Alexa 555 was added on the
237 left chambers at a concentration of 1 µM. For live cell imaging, neurons were prestained with
238 SP-DiOC$_{18}$(3) (3,3'-Dioctadecyl-5,5'-Di(4-Sulfophenyl)Oxacarbocyanine, Sodium
239 Salt). α-syn fibrils were analyzed by the Zeiss LSM 780 confocal microscope system. After
240 16 hours, media in each chamber was replaced with fresh media. The fluorescence intensities

JNeurosci Accepted Manuscript

were measured from the media by the microplate reader (Mithwas[2] LB 943, Berthold Technologies GmbH & Co. KG).

Plasmids

GCamp3-ML1 was kindly gifted from Haoxing Xu. The human ATP13A2 lentivirus was provided by Christopher Rochet. Lentiviruses carrying short hairpin plasmid RNA (shRNA) targeting human *SNCA* were purchased from Open Biosystems (GE Healthcare).

Western blotting

Immunoblotting was conducted as described previously (Tsunemi and Krainc, 2014, Tsunemi, et al., 2014). The antibodies used were anti human Lysosome-associated membrane protein (LAMP) 1 luminal domain (R&D), anti-human LAMP 1 (Santa Cruz Biotechnology), anti-human β-iii tubulin (Covance), and human Vimentin (BD Biosciences), anti-human GAPDH (Millipore), human ALIX (Santa Cruz), anti-human alpha synuclein C-20 (Santa Cruz), anti-human Huntingtin (Millipore), anti-human TDP43 (12892-1-AP, Proteintech), and anti-human tau (Dako), anti-human TH (Millipore), anti-human Tsg101 (GeneTex), and anti human CD63 (Developmental Studies Hybridoma Bank).

Mitochondrial respiration analysis

To measure mitochondrial respiration, we used Seahorse XF24, extracellular flux analyzer (Seahorse Bioscience) as described previously with minor modifications (Grunewald, et al., 2012). We plated 10,000 iPSCs per well at day 24 from the start of differentiation and added 1 μM oligomycin, 1.5 μM carbonylcyanide-p-trifluoromethoxyphenylhydrazone (FCCP) and 1 μM antimycin A for each time point. After analysis, remaining cells were harvested to measure protein levels, which were used for normalizing oxygen consumption rates.

Statistical analysis

All data were prepared for analysis with standard spreadsheet software (Microsoft Excel). Statistical analysis was performed by one-way ANOVA *post hoc* Tukey test or Student *t* test. All error bars represent SEM in figures.

Results

PARK9 patient DA neurons develop pathogenic phenotypes including lysosomal dysfunction and time-dependent α-synuclein accumulation

In order to investigate PARK9 function in neurons, we generated iPSC-derived dopaminergic (DA) neurons from healthy controls and *PARK9*-mutant KRS patients (Kriks et al., 2011, Mazzulli, et al., 2016a) which were positive for iPSC (Fig. 1-1) and DA neuronal markers (Fig. 1-2). Using time-dependent analysis of pathogenic phenotypes, we found that by early time points in culture (day 40 after differentiation), patient neurons already demonstrated defective exosome secretion (Fig. 1A) and lysosomal proteolysis (Fig. 1B). Moreover, lysosomal enzyme activity in the media was also significantly decreased in patient neurons indicative of impaired lysosomal exocytosis (Fig. 1C) (Medina et al., 2011).

JNeurosci Accepted Manuscript

284 Next, we examined whether this might disrupt α-syn processing, and indeed, found that patient
285 neurons exhibited decreased secretion of α-syn by day 40 both in the media (Fig. 1D) and in
286 exosomes (Fig. 1E). Importantly, these pathogenic phenotypes persisted until day 120 after
287 differentiation, including defective exosome secretion, lysosomal proteolysis, lysosomal
288 exocytosis and α-syn secretion (Fig. 1-3). Interestingly, α-syn accumulation occurs later in the
289 pathogenic process, potentially as a result of defective secretion and impaired lysosomal
290 degradation (Fig. 1F). As shown in Fig. 1-3F, Fig. 1GH, α-syn did not accumulate intracellularly
291 at early time points, with no observable increase in either soluble or insoluble α-syn levels at
292 day 60 (Fig. 1-3F), and only by day 90 did α-syn increase in the insoluble fraction (Fig. 1G), and
293 in the soluble fraction by day 120 (Fig. 1H). Thus, PARK9 patient neurons exhibit multiple
294 pathogenic phenotypes including defective α-syn secretion and its increased intracellular
295 accumulation.
296
297 **Defective α-synuclein secretion in *PARK9* patient DA neurons**
298 To further examine the mechanism of α-syn neuronal secretion, we cultured DA neurons in four
299 chambered microfluidic devices (Brahic et al., 2016) with top and bottom chambers connected
300 by 450 µm microgroove barriers, allowing for neurons cultured in the top two chambers to
301 extend their axons into the bottom two chambers (Fig. 2A). This system thus enabled us to
302 analyze α-syn release from axons compared to the cell body. DA neurons were cultured in the
303 top chambers 24 days after the start of differentiation (d24) (Fig. 2-1, A to C), with axons
304 extending through aligned microgrooves into the bottom chambers by day 60 (Fig. 2B). In order
305 to track α-syn transport in neurons, synthetic α-syn fibrils were generated and labeled with
306 Alexa-555 (α-syn 555) (Mazzulli, et al., 2011). Using trypan blue quenching assay, we confirmed
307 the internalization of α-syn 555 (Fig. 2-1D).
308
309 While the uptake of α-syn 555 was not significantly different between control and *PARK9*-
310 mutant DA neurons (Fig. 2-1, D and E), we found that *PARK9*-mutant DA neurons showed
311 significantly decreased total α-syn secretion from the cell body (top chamber media) as
312 compared to control neurons (Fig. 2C-left). Concomitantly, decreased secretion of α-syn
313 resulted in its gradual accumulation in the soma of *PARK9*-mutant DA neurons (Fig. 2D), which
314 lasted up to one week after fibril addition, as compared to control neurons, which had cleared
315 α-syn 555 by this time (Fig. 2E). Importantly, increasing *PARK9* expression with lentiviral-
316 mediated transduction resulted in increased secretion of α-syn (Fig. 2C-right) and its decreased
317 accumulation in the soma of *PARK9*-mutant DA neurons (Fig. 2, F and G). In contrast, when we
318 examined the axons of DA neurons, we found that the number of α-syn 555 puncta in axonal
319 terminals was significantly reduced in *PARK9*-mutant neurons (Fig. 2H), and could not be
320 rescued by fully lentiviral-mediated *PARK9* overexpression (Fig. 2I). Of note, α-syn secretion
321 from the axons of patient neurons was also significantly decreased as compared to control
322 neurons (Fig. 2J), potentially due to both decreased trafficking to the axons and defective
323 secretion. Together, these results suggest that defective α-syn secretion both from the cell
324 body and axons contributes to its gradual intracellular accumulation in patient neurons.
325
326 ***PARK9* patient DA neurons exhibit dysfunctional lysosomal Ca^{2+} homeostasis**

JNeurosci Accepted Manuscript

327 As secreted lysosomal enzyme activity was also decreased in *PARK9*-mutant neurons (Fig. 1C),
328 we next examined the potential mechanisms contributing to this defect. We first tested the
329 electrophysiological properties of PARK9-deficient DA neurons by conducting cell-attached
330 patch clamp recordings (Fig. 3A). We found that the rate of spontaneous firing was higher in
331 *PARK9*-mutant DA neurons compared to controls (Fig. 3, B to D). To determine if the PARK9
332 mutation affected intracellular Ca^{2+} levels, the ratiometric fluorescent dye Fura-2 AM was used
333 to measure cytosolic Ca^{2+} concentration (Dryanovski, et al., 2013, Shen et al., 2012). Basal
334 cytosolic Ca^{2+} levels were significantly higher in both PARK9 mutant fibroblasts (Fig. 3E) and
335 *PARK9* mutant DA neurons (Fig. 3F) at day 120. Importantly, lentivirus-mediated PARK9
336 overexpression (Fig. 3-1A,B) normalized abnormal Ca^{2+} levels (Fig. 3E, F).
337
338 As ATP13A2/PARK9 localizes to endolysosomes (Ramirez, et al., 2006, Tsunemi, et al., 2014), we
339 examined whether defective lysosomal Ca^{2+} handling might contribute to the elevation in
340 cytosolic Ca^{2+} concentration. First, we measured changes in free cytosolic Ca^{2+} levels upon GPN
341 (glycyl-L-phenylalanine 2-naphtylamide) treatment which induces lysosomal Ca^{2+} release (Fig. 3,
342 G to I). While 50 µM GPN significantly increased cytosolic Ca^{2+} levels in control fibroblasts, it
343 had no effect in either *PARK9*-mutant fibroblasts (Fig. 3, G and H) or DA neurons (Fig. 3I),
344 suggesting that lysosomal Ca^{2+} release or Ca^{2+} sequestration was impaired by PARK9 deficiency.
345 To address this question, we used a genetically encoded lysosomal sensor whose Ca^{2+} sensitive
346 fluorophore is positioned at the outer surface of the lysosome, allowing it to monitor efflux of
347 Ca^{2+} (GCaMP3-ML1) (Shen, et al., 2012). Bafilomycin A1 (Baf1) (200 nM) treatment (which
348 results in leakage of Ca^{2+} from lysosomes (Morgan et al., 2015)) led to a transient elevation in
349 GCaMP3-ML1 fluorescence (Fig. 3J), even after normalization for changes in lysosomal volume
350 (Usenovic, et al., 2012) (Fig. 3, K and L). We then depleted *PARK9* by shRNA (Tsunemi, et al.,
351 2014) (Fig. 3-1) and found that Baf1-induced lysosomal Ca^{2+} release as measured by GCaMP3-
352 ML1 was significantly reduced compared to control cells (scramble shRNA) (Fig. 3L, M, Fig. 3-
353 1C). Similar results were observed in PARK9-deficient fibroblasts compared to controls and
354 lentivirus-mediated PARK9 overexpression restored the impaired Ca^{2+} release (Fig. 3H, I, N). We
355 then asked whether this defect in lysosomal Ca^{2+} release was caused by impaired lysosomal Ca^{2+}
356 storage in *PARK9*-deficient cells. To this end, Rhod dextran was used to estimate luminal
357 lysosomal Ca^{2+} levels (Lloyd-Evans et al., 2008). In control fibroblasts, Rhod dextran
358 fluorescence was robust and rapidly decreased upon Baf1 treatment. In contrast, in *PARK9*-
359 mutant fibroblasts, Rhod dextran fluorescence was weak and was not significantly altered after
360 Baf1 treatment (Fig. 3O), consistent with the proposition that PARK9 deficiency leads to
361 decreased lysosomal Ca^{2+} storage (Fig. 3P).
362
363 **PARK9 regulates lysosomal exocytosis via modulation of lysosomal Ca^{2+} homeostasis**
364 Recent studies have shown that high lysosomal Ca^{2+} concentrations are necessary to trigger
365 trafficking and exocytosis (Xu and Ren, 2015). Lysosomal exocytosis involves lysosomal fusion
366 with the plasma membrane, resulting in the release of contents into the extracellular space
367 (Samie and Xu, 2014). Consistent with what we observed in *PARK9* patient neurons (Fig. 1C),
368 lysosomal GCase activity in the media was significantly decreased in *PARK9* patient fibroblasts
369 (Fig. 3Q). To determine whether this change in enzymatic activity in the media was driven by
370 lysosomal exocytosis, control cells were treated with 50 µM GPN which has been shown to

JNeurosci Accepted Manuscript

371 drive lysosomal exocytosis, resulting in an increase in GCase activity in the media (Fig. 3Q).
372 Importantly, this was inhibited by the intracellular Ca^{2+} chelator BAPTA, confirming that
373 lysosomal exocytosis requires a rapid increase in Ca^{2+} concentration near the lysosomal surface
374 (Xu and Ren, 2015). In contrast, treatment with thapsigargin, an inhibitor of the
375 sarco/endoplasmic reticulum Ca^{2+} ATPase which induces Ca^{2+} release from the ER, did not
376 disrupt GCase activity in the media, further confirming the importance of lysosomal Ca^{2+} release
377 for activation of lysosomal exocytosis (Raffaello et al., 2016) (Fig. 3R). To further confirm a role
378 for PARK9 in regulating lysosomal exocytosis, we measured the enzymatic activity of several
379 lysosomal enzymes in the media that is normalized to their activity in cell lysate. The media
380 activity of GCase, β-hexosaminidase and acid phosphatase released from *PARK9*-mutant
381 fibroblasts were all significantly decreased compared to that from control fibroblasts (Fig. 4, A
382 to C), suggesting decreased secretion of lysosomal hydrolases due to *PARK9* deficiency.
383 Conversely, increased expression of *PARK9* (Fig. 3-1C) led to increased lysosomal enzymatic
384 activity in the media (Fig. 4, D to F), indicating an active involvement of PARK9 in this pathway.
385
386 To further assess PARK9's role in lysosomal exocytosis, we conducted LAMP-1 cell-surface
387 staining (Fig. 4, G and H) with an antibody against human LAMP-1 topological domain (luminal
388 domain) which is exposed to the cell surface upon lysosomal exocytosis after lysosomes fuse
389 with the plasma membrane. At steady-state conditions (before treatment), LAMP-1 was not
390 present on the cell surface but subsequently translocated to the cell surface upon Baf1
391 treatment. In contrast, *PARK9* silencing inhibited Baf1-induced LAMP-1 translocation to the cell
392 surface, while increased *PARK9* levels enhanced its translocation (Fig. 4G). In addition, we
393 investigated LAMP-1 translocation biochemically by conducting a cell surface biotinylation assay
394 through which proteins on the plasma membrane are biotinylated and collected by
395 streptavidin-beads (Fig. 4, I and J). After enhanced or silenced *PARK9* expression levels, we
396 treated cells with 200 nM Baf1 for up to 2 hours and subjected their lysates to precipitation by
397 streptavidin beads. Both cell lysates and precipitated proteins were subsequently analyzed by
398 immunoblotting with LAMP-1 antibodies (Fig. 4I) and examined for the time course of LAMP-1
399 translocation to the cell surface after Baf1 treatment (Fig. 4J). Importantly, while increased
400 *PARK9* expression led to increased LAMP-1 on the cell surface, *PARK9* silencing decreased its
401 translocation (Fig. 4, I and J), further demonstrating that PARK9 levels regulate LAMP-1
402 translocation during lysosomal exocytosis.
403
404 **Upregulation of lysosomal exocytosis with lysosomal Ca^{2+} channel TRPML1 agonists rescues**
405 **α-synuclein secretion defects and intracellular accumulation in *PARK9* patient DA neurons**
406 TRPML1 is the main Ca^{2+} channel responsible for Ca^{2+} release from lysosomes and the TRPML1
407 agonist, ML-SA1, has been shown to induce lysosomal exocytosis (Shen, et al., 2012). We thus
408 examined whether we could rescue deficient lysosomal exocytosis in *PARK9*-mutant fibroblasts
409 using three different TRPML1 agonists: ML-SA1, SF-22 and MK6-83. We found that all three
410 agonists increased lysosomal exocytosis, as measured by a significant increase in the
411 extracellular lysosomal enzymatic activity of GCase (normalized to intracellular activity levels) in
412 both control and *PARK9*-mutated fibroblasts in a dose dependent manner (Fig. 5A, Fig. 5-1A)
413 (Chen et al., 2014). As a result, intracellular GCase activities were decreased (Fig. 5-1B). This
414 was further confirmed using LAMP-1 cell surface staining, which demonstrated high cell surface

JNeurosci Accepted Manuscript

415 staining upon MK6-83 agonist treatment (Fig. 5B - top), but was abolished by *PARK9* silencing
416 (Fig. 5B- bottom), further indicating that PARK9 is also involved in TRPML1-induced lysosomal
417 exocytosis. We confirmed the specificity of these TRPML1 agonists by examining the effect of
418 TRPML1 inhibition on TRPML1 agonist-mediated GCase release. Genetic depletion by shRNA of
419 TRPML1 was confirmed by immunoblotting (Fig. 5-1C). Pharmacological inhibition of TRPML1
420 was achieved by adding either 10 mM adenosine or 100 nM $LaCl_3$ in the culture media one hour
421 before TRPML1 activation (Dong et al., 2009, Zhong et al., 2017). Importantly, TRPML1
422 inhibition either by pretreatment with either shRNA-mediated TRPML1 silencing or TRPML1
423 inhibitors, adenosine and La^{3+}, rendered the cells insensitive to the TRPML1 agonist,
424 demonstrating the direct effect of the TRPML1 agonist on TRPML1 channels (Fig. 5-1D). We
425 further tested whether the Ca^{2+} storage deficit in *PARK9*-mutant lysosomes resulted from
426 overactivation of TRPML1, by examining the effect of TRPML1 inhibition on lysosomal Ca^{2+}
427 release mediated by Baf1, which is the most potent inducer of lysosomal exocytosis (Fig. 3Q).
428 We found that either genetic TRPML1 silencing or chemical inhibition of TRPML1 reduced Ca^{2+}
429 release from lysosomes in control fibroblasts, suggesting the contribution of TRPML1 on
430 lysosomal Ca^{2+} release (Fig. 5-1E). In contrast, these treatments did not show any effects on
431 *PARK9*-mutant cells (Fig. 5-1F), demonstrating that inhibition of TRPML1 does not disrupt
432 impaired Ca^{2+} release from *PARK9*-mutant lysosomes. Lysosomal exocytosis was increased
433 either by PARK9 overexpression (Fig. 4) or by TRPML1-agonists, both of which became
434 ineffective when lysosomal Ca^{2+} was chelated in advance (Fig. 5-1G, Fig. 3Q). Together, these
435 results suggest that decreased lysosomal exocytosis by ATP13A2 deficiency would be largely
436 due to a decrease in lysosomal Ca^{2+}.
437
438 Then, we examined if impaired α-syn secretion could be rescued by upregulating lysosomal
439 exocytosis with TRPML1 agonists. Importantly, treatment with any of the three TRPML1
440 agonists ML-SA1, SF-22 or MK6-83 for 24 hours was sufficient to increase α-syn secretion (Fig.
441 5C), and concomitantly reduced intracellular α-syn levels (Fig. 5, D and E) from both control and
442 *PARK9*-mutant DA neurons (Fig. 5F). Moreover, this significantly decreased α-syn intracellular
443 accumulation in both Tx soluble and SDS soluble fractions in *PARK9*-mutant DA neurons (Fig. 5,
444 G to I). Finally, we examined mitochondrial respiration in *PARK9*-mutant DA neurons to
445 examine if TRPML1 agonist treatment could rescue any mitochondrial deficits (Fig. 5J). *PARK9*-
446 mutant DA neurons exhibited increased in all phases of mitochondrial activities; basal
447 respiration from 0 to 17 min , ATP production from 26 to 43 min, and maximum respiration
448 from 52 to 69 min, which are considered as a response to high energy demand from cellular
449 organelles including lysosomes and consistent with previous studies (Grunewald, et al., 2012).
450 Importantly, the TRPML1 agonist (1 uM MK6-83) normalized this activity back to the level of
451 control neurons. Because TRPML1 agonists are unlikely to have direct effects on mitochondria,
452 our data suggest that this could be the result of improved Ca^{2+} homeostasis, which enhances
453 lysosomal exocytosis and a-syn secretion. Taken together, these results highlight a key role for
454 upregulating lysosomal exocytosis as an effective pathway for regulating α-syn levels by
455 increasing its secretion and decreasing its intracellular accumulation in a human DA neuron
456 model of synucleinopathy, and further demonstrate that this pathway is defective in *PARK9*
457 patient neurons due to misregulation of lysosomal Ca^{2+} dynamics.
458

JNeurosci Accepted Manuscript

459 **Discussion**
460 The accumulation of misfolded proteins is a common pathological feature of many
461 neurodegenerative disorders (Eisele et al., 2015). Lewy bodies and neurites (LN) are a
462 pathological hallmark of Parkinson's disease, demonstrating a critical role for α-syn
463 accumulation (Lang and Lozano, 1998) and modulation of α-syn levels in Parkinson's
464 pathogenesis (Rubinsztein, 2006). By examining a monogenic form of PD, ATP13A2/PARK9, we
465 found that lysosomal exocytosis is an important pathway that regulates α-syn levels in human
466 neurons. PARK9-deficiency impaired this pathway resulting in both lysosomal dysfunction and
467 α-syn accumulation. Restoration of lysosomal exocytosis by TRPML1 agonists was able to
468 improve lysosomal exocytosis and reduce α-syn levels in patient DA neurons.
469
470 Lysosomal exocytosis is a critical pathway whereby lysosomes fuse with the plasma membrane
471 and expel their storage materials outside of the cells (Xu and Ren, 2015). This unconventional
472 exocytotic pathway was initially discovered by studying the protozoan parasite *Trypanosoma*
473 *cruzi* (Tardieux et al., 1992); follow-up work revealed that this process exists in many cell types
474 and is required to repair injured plasma membrane (Reddy et al., 2001). We found that PARK9
475 was able to directly regulate lysosomal exocytosis which plays an important role in modulating
476 α-syn intracellular levels. In contrast, exosomal secretion only makes a modest contribution to
477 the secretion of α-syn (Tsunemi, et al., 2014). Of note, upregulating lysosomal exocytosis may
478 be beneficial not only for *PARK9* DA neurons, but also other disorders including lysosomal
479 storage diseases (Medina, et al., 2011, Shen, et al., 2012) and Alzheimer's disease (Bae et al.,
480 2014), as this pathway can reduce the levels of both soluble and insoluble protein aggregates
481 contributing to these diseases.
482
483 α-syn is predominantly found in presynaptic terminals of healthy neurons and has a putative
484 role in synaptic transmission (Burre et al., 2010). However, once its abundance exceeds a
485 certain threshold level, a-syn becomes toxic (Wong and Krainc, 2017). Our results suggest that
486 the exocytotic pathway is indispensable for neurons to reduce α-syn levels. Indeed, α-syn is
487 continuously secreted even under physiological conditions as it is found in the cerebrospinal
488 fluid (CSF) of both PD patient and healthy controls (Borghi et al., 2000). While neurons can
489 degrade a-syn in several ways, when these mechanisms are overwhelmed, they may utilize
490 secretory pathways as a last resort to reduce toxic protein accumulation (Rubinsztein, 2006). In
491 this situation, PARK9-deficiency could lead to accumulation of potentially toxic levels of α-syn
492 (Usenovic, et al., 2012) (Tsunemi, et al., 2014).
493
494 Using Ca^{2+} sensors targeted to cytosolic and lysosomal compartments, we found that a PARK9
495 deficiency results in elevated cytosolic and reduced lysosomal Ca^{2+} concentration. Normally,
496 lysosomes maintain an intraluminal Ca^{2+} concentration (~0.5 mM) that is similar to those of the
497 endoplasmic reticulum or mitochondria, both of which have been established as intracellular
498 Ca^{2+} stores (Raffaello, et al., 2016). However, in contrast to these organelles, the mechanisms
499 by which Ca^{2+} is transported into acidic vesicles is still not well understood (Raffaello, et al.,
500 2016). Our results indicate that PARK9 may play a significant role in the sequestration of Ca^{2+} in
501 lysosomes. Interestingly, deficits in PARK9 function led to an elevation in cytosolic Ca^{2+}
502 concentration. Previous work has linked elevated cytosolic Ca^{2+} levels to selective neuronal

JNeurosci Accepted Manuscript

503 vulnerability in PD. In particular, Ca^{2+} entry through Cav1 (L-type) Ca^{2+} channels during
504 autonomous spiking, stimulates mitochondrial respiration and oxidative stress in at-risk
505 neurons, like dopaminergic neurons in the substantia nigra, noradrenergic neurons in the locus
506 coeruleus and cholinergic neurons in the dorsal motor nucleus of the vagus (Surmeier et al.,
507 2017). Deficits in PARK9-mediated sequestration of Ca^{2+} in lysosomes may further increase the
508 cytosolic Ca^{2+} loading in these cell types, adding to mitochondrial oxidant stress. It remains to
509 be determined whether the increased spiking rate in *PARK9*-mutant DA neurons is an attempt
510 to compensate for the deficit in lysosomal Ca^{2+} storage (by increasing the availability of Ca^{2+} to
511 be pumped into the lysosome) or is an inadvertent by-product of the failure to adequately
512 sequester Ca^{2+} in lysosomes. In either case, the PARK-9 mutation adds to the Ca^{2+} burden on DA
513 neurons and their vulnerability.
514
515 In conclusion, we show that intracellular α-syn levels can be regulated by PARK9-mediated
516 lysosomal exocytosis. Disruption of these pathways evokes a series of cellular dysfunctions
517 observed in *PARK9*-mutant DA patient neurons, whereas restoring lysosomal exocytosis
518 decreases pathology by decreasing intracellular levels of α-syn via its secretion. Targeting
519 secretory pathway may thus be an important therapeutic strategy for ameliorating α-syn
520 accumulation across multiple synucleinopathies including Parkinson's.
521 (681 words)
522
523
524 **Acknowledgments: Funding**: This work is supported by National Institute of Health (R37
525 NS096241) to DK and JSPS KAKENHI Grants (16H07185) and (18K07510); Brains research
526 foundation; Juntendo University Research Institute for Diseases of Old Age and Environmental
527 & Gender-specific Medicine to T.T. **Author contributions**: D.K. and T.T. organized the project,
528 interpreted the results and wrote the manuscript. T.T., S. J., K. H., M. S., A.Y., T.P., W.A., J.R.M.,
529 Z.X. and Y.I. performed experiments. Y. W., D.J.S. and N.H. provided helpful suggestions and
530 helped with data interpretation and writing of the manuscript. **Competing interests**: The
531 authors declare that they have no competing interests.
532

JNeurosci Accepted Manuscript

533 **Figures**:

534 **Fig. 1**. ***PARK9* patient DA neurons develop pathogenic phenotypes including lysosomal**
535 **dysfunction and time-dependent α-synuclein accumulation**

536

537 (**A**) The number of exosomes secreted from four control and two *PARK9*-mutant DA neurons
538 were analyzed at day 40 after the initiation of differentiation. The number of exosomes was
539 normalized by total protein in cell lysates (n = 3, **p* = 0.0001). (**B**) Lysosomal proteolysis
540 measured by radioactive pulse chase in four control and two *PARK9*-mutant DA neurons at day
541 40 after the initiation of differentiation (n = 3, **p* = 0.0001). (**C**) β-glucocerebrosidase (GCase)
542 activity in the secreted media taken from four control and two *PARK9*-mutant DA neurons at
543 day 40 after the initiation of differentiation. The activity in the media was normalized by the
544 activity in cells and shown as a percentage of control 1 (n = 3, **p* = 0.0001). (**D**) Enzyme-Linked
545 Immunosorbent Assay (ELISA) to quantify α-syn in the media taken from four control and two
546 *PARK9*-mutant DA neurons at day 40 after the initiation of differentiation (n = 3, **p* = 0.0001).
547 (**E**) The α-syn ELISA for detecting α-syn proteins in exosomes taken from four control and two
548 *PARK9*-mutant DA neurons at day 40 after the initiation of differentiation (n = 3, **p* = 0.0001).
549 (**F**) The sequential pathological cascade observed in long-term cultures of iPS-derived *PARK9* DA
550 neurons. (**G to I**) Immunoblot analysis of α-syn proteins in four control, two *PARK9*-mutant and
551 *SNCA* triplication DA neurons Day 90 (**G**) and Day 120 (**H**) after the initiation of differentiation.
552 After normalization to β-iii-tubulin, the relative α-syn levels are shown as fold changes
553 compared with control 1 (n = 3, **p* = 0.0087, ***p* = 0.0001, ****p* = 0.004). The statistical
554 analysis was conducted using one-way ANOVA Tukey *post hoc* test unless otherwise stated.

555

556 **Fig. 2. Defective α-synuclein secretion from both the soma and axons in *PARK9* patient DA**
557 **neurons**

558

559 (**A**) A schematic image of a microfluidic device in which two sets of chambers are connected
560 through 450 μm microgroove groove. Neurons were cultured in the top chambers and extend
561 their axons through grooves into the bottom chambers. (**B**) Representative images of DA
562 neurons cultured with Alexia555 labeled α-syn fibrils in microfluidic devices. DA neurons were
563 stained with β-iii-tubulin and visualized as α-syn fibrils conjugated with Alexa 555. A merged
564 image is shown at right. (**C**) Fluorescence intensities in the media taken from the top chambers
565 of microfluidic devices. DA neurons were infected with empty lentivirus (**left**) or lentivirus
566 expressing human *PARK9* (**right**) (n = 3, **p* = 0.0276, ***p* = 0.0001, ****p* = 0.0001). After
567 culturing in media containing α-syn fibrils for 24 hours, media was changed to fresh media.
568 After 24 hours, the media was collected and fluorescence intensities were analyzed. (**D**)
569 Fluorescence intensities of α-syn fibrils in three control and two *PARK9* DA mutant neurons.
570 After culturing in media containing α-syn fibrils for 24 hours, the media was replaced with fresh
571 media. The fluorescence intensities were measured at 24, 36, 48 and 60 hours (n = 3, **p* =
572 0.0158, ***p* = 0.0265). (**E**) Representative images of DA neurons (Cont 1 and Mut 1) cultured in
573 media containing Alexia555 labeled α-syn fibrils for 24 hours and subsequently cultured in fresh
574 media for a week. (**F**) Representative images of *PARK9*-mutant DA neurons (Mut 1) transfected
575 with empty lentivirus (top) or *PARK9* expressing lentivirus (bottom) and subsequently cultured

JNeurosci Accepted Manuscript

576 with Alexia555 labeled α-syn fibrils. (**G**) The quantification of total α-syn fluorescence intensity
577 in DA neurons (n = 3, **p* = 0.0350, ***p* = 0.0255, Student *t* test). (**H**) Representative images of
578 the axons of control (top) and *PARK9*-mutant (bottom) DA neurons in the bottom chambers of
579 microfluidic devices after adding α-syn fibrils to the top chamber. Arrows show α-syn fibrils. (**I**)
580 The number of α-syn fibrils were counted in each axon of four control and two mutant DA
581 neurons (n = 10-20, **p* = 0.0106, ***p* = 0.0354). (**J**) Fluorescence intensities in the media taken
582 from the bottom chambers of the microfluidic devices. DA neurons were infected with empty
583 lentivirus (**left**) or lentivirus expressing human *PARK9* (**right**) (n = 3, **p* = 0.0016, ***p* = 0.0354,
584 ****p* = 0.0001). After culturing in media containing α-syn fibrils for 24 hours, the media was
585 changed to fresh media for another 24 hours before the media was collected and fluorescence
586 intensities were analyzed (n = 3, $*p < 0.05$). The statistical analysis was conducted using one-
587 way ANOVA Tukey *post hoc* test unless otherwise stated. Scale bars represent 200 μm for
588 Figure **B**; 50 μm for Figure **D**, **E** and **F**; 10 μm for Figure **H**.
589
590 **Fig. 3. *PARK9* patient DA neurons exhibit dysfunctional lysosomal Ca^{2+} homeostasis**
591
592 (**A to D**) Spontaneous firing rate of DA neurons taken from control and *PARK9* patients. (**A**)
593 Representative images of DA neurons from control individuals (left), *PARK9* patients (right)
594 during cell-attached patch clamp recordings. (**B**) Representative cell-attached recordings from
595 control (top) and *PARK9* patient-derived neurons (bottom). (**C**) Box plots showing the
596 distribution of spiking rates in control (N=10) and *PARK9* DA (N=10) neurons (control
597 median=4.61 Hz vs. *PARK9* median= 7.25 Hz; **p* = 0.021, unpaired T-test with Welch's
598 correction). (**D**) Box plots showing the distribution of coefficient of variation in control (N=10)
599 and *PARK9* DA (N=10) neurons (control median=6.1 vs. *PARK9* median= 4.2; **p* = 0.1051, Mann-
600 Whitney). (**E and F**) Cytosolic Ca^{2+} levels were measured using Fura-2 AM Ca^{2+} indicator. The
601 intracellular Ca^{2+} concentration was measured in two control, two *PARK9*-mutant fibroblasts
602 and two *PARK9*-mutant fibroblasts that were transfected with lentivirus expressing PARK9. (**E**)
603 and in iPSC-derived dopaminergic (DA) neurons (**F**) (n = 10, **p* = 0.0001). (**G to I**) Ca^{2+} release
604 from control and *PARK9*-mutant fibroblasts and DA neurons. (**G**) The change of cytosolic Ca^{2+}
605 concentration by GPN (glycyl-L-phenylalanine 2-naphtylamide) treatment was monitored by
606 Fura-2 fluorescence ratios at 340 nm/380 nm. (**H**) Fura-2 fluorescence ratios were shown
607 before and after GPN treatment in two controls and two *PARK9*-mutant fibroblasts (n = 10, **p* =
608 0.002). (**I**) Ca^{2+} release from lysosomes was decreased in *PARK9*-mutant DA neurons. Fura-2
609 ratios were measured before and after GPN treatment (n = 10, **p* = 0.0001). (**J to N**) Ca^{2+}
610 release from lysosomes was analyzed with the lysosome targeted Ca^{2+} sensor, GCamP3-ML1. (**J**)
611 Representative images of GCamp3-ML1 expressing H4 cells that were labeled with LAMP-1
612 before and after Baf1 treatment. (**K**) GCamp3-ML1 and Lysotracker intensities were monitored
613 during Baf1 treatment. (**L**) The ratios of green (GCamp3-ML1) to red fluorescence (Lysotracker
614 Red) were monitored during Baf1 treatment. (**M**) The ratios of green to red fluorescence under
615 Baf1 treatment were analyzed in H4 cells transfected with Scrb shRNA or shRNA against human
616 *PARK9* (n = 30 to 50/cells, **p* = 0.0005, ***p* = 0.0422, ****p* = 0.0303, *****p* = 0.0063). (**N**) The
617 ratios of green to red fluorescence under Baf1 treatment were analyzed in control and *PARK9*-
618 mutant fibroblasts and two *PARK9*-mutant fibroblasts that were transfected with lentivirus
619 expressing PARK9. (n = 30 to 50/cells, , **p* = 0.0001). (**O and P**) Ca^{2+} levels in lysosomes were

JNeurosci Accepted Manuscript

620 measured using Ca^{2+} dye, Rhod dextran. (**O**) Representative images of control and mutant
621 fibroblasts labeled with Rhod dextran and Cascade blue. (**P**) Quantification of Rhod dextran and
622 Cascade blue fluorescence intensities before and after Baf1 treatment in control and *PARK9*-
623 mutant fibroblasts (n = 10 cells, *p = 0.0001, Student t test). (**Q**) The effect of PARK9-deficiency
624 on Ca^{2+} dependent lysosomal exocytosis. GCase activity was measured in the media before and
625 after 50 μM GPN or 200 nM Baf1 treatment. The treatment of Ca^{2+} chelator, 1,2-bis(*o*-
626 aminophenoxy)ethane-*N*,*N*,*N'*,*N'*-tetraacetic acid (BAPTA) diminished the effect of GPN and
627 Baf1 (n = 3, *p = 0.0135, **p = 0.0442, ***p = 0.0008, $^{\#}p$ = 0.0347, $^{\#\#}p$ = 0.0023). (**R**) The effect
628 of Ca^{2+} release from the endoplasmic reticulum (ER) on lysosomal exocytosis was analyzed.
629 GCase activity was measured from the media of two control or two *PARK9*-mutant fibroblasts
630 before (left) and after 2 μM thapsigargin treatment (right) (n = 3, p = 0.95). The statistical
631 analysis was conducted using one-way ANOVA Tukey *post hoc* test unless otherwise stated.
632 Scale bars represent 20 μm for Figure **J**, **O**.
633
634 **Fig. 4. PARK9 regulation of lysosomal exocytosis**
635
636 (**A to C**) Activities of three lysosomal acid hydrolases in media were measured in *PARK9*-mutant
637 and control fibroblasts. (**A**) GCase activity in media normalized to activity in cell lysates (n = 3,
638 *p = 0.0103, **p = 0.0093). (**B**) β-hexosaminidase activity in media normalized to activity in cell
639 lysates (n = 3, *p = 0.0417, **p = 0.0462). (**C**) Acid phosphatase activity in media normalized to
640 activity in cell lysates (n = 3, *p = 0.0279, **p = 0.0181). (**D to F**) Activities of lysosomal acid
641 hydrolases released into media were increased in *PARK9* overexpressing H4 cells. (**D**) GCase
642 activity in media normalized to activity in cell lysates (n = 3, *p = 0.036, Student t test). (**E**) β-
643 hexosaminidase activity in media normalized to activity in cell lysates (n = 3, *p = 0.0101,
644 Student t test). (**F**) Acid phosphatase activity in media normalized to activity in cell lysates (n =
645 3, *p = 0.0111, Student t test). (**G**) LAMP-1 surface staining in *PARK9*-knockdown and *PARK9*-
646 overexpressing H4 cells. LAMP-1 expression (green fluorescence) on the plasma membrane
647 marked by Dil (red fluorescence) was visualized at steady-state (**upper**) and after 30 min
648 Bafilomycin A1 (Baf1) treatment (**upper middle**). LAMP-1 expression on the plasma membrane
649 was also visualized in *PARK9*-silenced H4 cells with Baf1 treatment (**lower middle**) and *PARK9*-
650 overexpressing H4 cells with Baf1 treatment (**bottom**). (**H**) Fluorescence intensity ratios (LAMP-
651 1/Dil) are shown (n = 3, *p = 0.0001, **p = 0.0002, Student t test). (**I**) Cell surface biotinylation
652 assay to analyze the effect of *PARK9* expression levels on Baf1-induced cell-surface LAMP1.
653 While overexpression of *PARK9* lead to increased expression, depletion of *PARK9* resulted in
654 reduced LAMP1 expression on the cell surface.
655 (**J**) The quantification of biotinylated LAMP1 proteins against total LAMP-1 proteins (n = 3, *p =
656 0.0005, **p = 0.0021, ***p = 0.0034, Student t test). The statistical analysis was conducted
657 using one-way ANOVA Tukey *post hoc* test unless otherwise stated. Values are mean ± SEM.
658 Scale bars represent 20 μm for Figure **G**.
659
660 **Fig. 5. Ca^{2+}-dependent lysosomal exocytosis rescues α-synuclein secretion in *PARK9* patient**
661 **DA neurons**
662

JNeurosci Accepted Manuscript

663 (**A**) The effect of transient receptor potential mucolipin 1 (TRPML1) channel agonists on
664 lysosomal exocytosis was analyzed in control and *PARK9*-mutant fibroblasts. The extracellular
665 and intracellular GCase activities were measured before and after 20 μM ML-SA1, 1 μM SF-22
666 and 1 μM MK6-83 treatments (n = 3, **p* = 0.0103, ***p* = 0.0045, ****p* = 0.0054, ****p* = 0.0106,
667 $^{\#}p$ = 0.0270, $^{\#\#}p$ = 0.0444, $^{\#\#\#}p$ = 0.0002). (**B**) The effect of TRPML1 channel agonist (20 μM ML-
668 SA1) on LAMP1 surface staining in H4 cells transfected with Scrb shRNA (**top**) or shRNA against
669 *PARK9* transfected (**bottom**). DiI was used as a plasma membrane marker. (**C**) α-syn levels from
670 the media taken from H4 cells measured by highly sensitive ELISA (n = 3, **p* = 0.0348, ***p* =
671 0.0011). (**D**) Immunoblot analysis of α-syn levels in H4 cells after treatment with DMSO, ML-
672 SA1, SF-22 or MK6-83 for 24 hours. (**E**) Quantification of α-syn levels was shown. After
673 normalization to GAPDH, the relative α-syn levels in treated cells were divided by α-syn levels in
674 cells treated with DMSO (leftmost) (n = 3, **p* = 0.0133, ***p* = 0.0077, ****p* = 0.0046). (**F**) α-syn
675 levels from the media taken from control or *PARK9*-mutant DA neurons measured by highly
676 sensitive ELISA (n = 3, **p* = 0.0001). (**G**) Immunoblot analysis of α-syn levels in DA neurons at
677 day 90 after treatment with DMSO, ML-SA1, SF-22 or MK6-83 for 24 hours.
678 (**H and I**) Quantification of α-syn levels. After normalization to β-iii-tubulin (**H.** Tx soluble
679 fraction) or Vimentin (**I.** SDS soluble fraction), the relative α-syn levels in the treated cells were
680 normalized to α-syn levels before treatment (green bars) (**H.** n = 3, **p* = 0.0415, ***p* = 0.0221,
681 ****p* = 0.0011, *****p* = 0.0001, **I.** n = 3, **p* = 0.0071, ***p* = 0.0006).
682 (**J**) Mitochondrial respiration analysis using two control, two *PARK9*-mutant DA neurons and
683 two *PARK9*-mutant DA neurons that are pretreated with 1 μM MK6-83 (n = 3, **p* = 0.0303)
684 The statistical analysis was conducted using one-way ANOVA Tukey *post hoc* test.
685 Scale bars represent 20 μm for Figure **B**.
686
687

JNeurosci Accepted Manuscript

688 **Supporting Information**
689
690 **Extended Data**
691 ***Immunofluorescence analysis***
692 DA Neurons and iPSCs were fixed in 4% formaldehyde and permeabilized /blocked with 0.3%
693 Triton X-100 or 0.2% saponin in 1% BSA with 4% normal goat serum in PBS for 20 min. The
694 following primary antibodies were used: anti β-iii-tubulin (Covance, #MMS-435P, 1:1000 or
695 Covance, #MRB-435P, 1:1000), tyrosine hydroxylase (EMD Millipore, #657012, 1:1000), HNF-3
696 beta (FOXA2) (Santa Cruz, #sc-101060, 1:100), LMX1a (EMD Millipore, #AB10533, 1:1000),
697 SSEA4 (EMD Millipore, #MAB4304, 1:100), TRA-1-60 (EMD Millipore, #MAB4360, 1:50), TRA-1-
698 81 (EMD Millipore, #MAB4381, 1:50), OCT4 (Abcam, #ab19857, 1:300), NANOG (Abcam,
699 #ab80892, 1:1000), AFP (Sigma Aldrich, #A8452, 1:100), SMA (Dako, #M0851, 1:100), α-Tubulin
700 (Sigma, T5168, 1:2000), TRPML1 (Alamone lab, ACC-081, 1:1000). The specimens were
701 incubated overnight, washed in PBS three times and incubated with Alexa-conjugated anti-
702 rabbit or anti-mouse antibodies at 1:400. For quantification, 10,000 cells were plated in one
703 well of 96-well plates and fluorescence intensities were measured and normalized by nuclear
704 staining (DAPI)
705
706 ***RNA extract and real-time PCR***
707 RNA extraction from H4 cells, fibroblast or DA neurons and real-time PCR were conducted as
708 described previously (Tsunemi and Krainc, 2014).
709
710 **Extended Figures**
711 **Fig. 1-1. Characterization of iPSCs**
712 **Fig. 1-2. Characterization of human iPSC-derived DA neurons**
713 **Fig. 1-3. Pathogenic phenotypes of *PARK9* patient DA neurons over time**
714 **Fig. 2-1. iPSC-derived DA neurons on microfluidics**
715 **Fig. 3-1. Modulation of *PARK9* expression levels**
716 **Fig. 5-1. The effect of TRPML1 agonists on lysosomal exocytosis**
717
718
719 **Fig. 1-1. Characterization of iPSCs**
720
721 (**A**) Immunocytochemistry for pluripotency markers SSEA4, TRA-1-60, TRA-1-81, OCT4 and
722 NANOG.
723 (**B**) Images of chromosome G-banding analysis of control (Cont 4) and mutant (Mut 1) iPSCs. (**C**)
724 Expression of three germ layer-specific markers after spontaneous differentiation. Markers of
725 ectodermal progenitor cells (β-iii-tubulin), endodermal lineage cells (α-fetoprotein) and
726 mesodermal lineage cells (SMA) were used.
727 (**D**) Direct sequence results of two *PARK9* mutant iPSC lines.
728 (**E**) Gene copy analysis for *SNCA* in Cont 1, Cont 2, Triplication and Mut 1.
729 Scale bars represent 50 μm for Figure **A** and 50 μm for Figure **C.**
730

JNeurosci Accepted Manuscript

731
732 **Fig. 1-2. Characterization of human iPSC-derived DA neurons**
733
734 (**A**) DA neurons analyzed by immunocytochemistry using FOXA2 (red) and tyrosine hydroxylase
735 (TH) (green) at day 60 after the initiation of differentiation. Percentage of cells expressing both
736 FOXA2 and TH during differentiation and maturation (n = 30-50).
737 (**B**) DA neurons analyzed by immunocytochemistry using Lmx1a (red) and tyrosine hydroxylase
738 (TH) (green) at day 60 after the initiation of differentiation. Percentage cells expressing both
739 LMX1a and TH during differentiation and maturation (n = 30-50).
740 (**C**) DA neurons analyzed by immunocytochemistry using β-iii-tubulin (β-iii-tub) (red) and
741 tyrosine hydroxylase (TH) (green) at day 60 after the initiation of differentiation. Percentage
742 cells expressing both β-iii-tubulin and TH during differentiation and maturation (n = 30-50).
743 Scale bars represent 100 μm.
744
745 **Fig. 1-3. Pathogenic phenotypes of *PARK9* patient DA neurons over time**
746
747 (**A**) The number of exosomes secreted from four control and two *PARK9*-mutant DA neurons
748 were analyzed at day 60, 90, 120 after the initiation of differentiation. The number of exosomes
749 was normalized to the total protein level from cell lysates (n = 3, *p = 0.0002, **p = 0.0276).
750 (**B**) Lysosomal proteolysis measured by radioactive pulse chase in four controls and two *PARK9*-
751 mutant DA neurons at day 60, 90, 120 after the initiation of differentiation. Data are shown as
752 fold changes normalized to control 1 at day 40 (n = 3, *p = 0.0001, **p = 0.0113, ***p =
753 0.0155).
754 (**C**) Released GCase activity in the media taken from four control and two *PARK9*-mutant DA
755 neurons at Day 60, 90, 120 after the initiation of differentiation. Activity in the media were
756 normalized to the activity in cell lysates, and shown as a percentage of control 1 at day 40 (n =
757 3, *p = 0.0001, **p = 0.0202, ***p = 0.0250).
758 (**D**) Enzyme-Linked Immunosorbent Assay (ELISA) to quantify α-syn protein levels in the media
759 taken from four control and two *PARK9*-mutant DA neurons at day 60, 90, 120 after the
760 initiation of differentiation (n = 3, *p = 0.0001, **p = 0.0001).
761 (**E**) α-syn ELISA for detecting α-syn protein levels in exosomes taken from four control and two
762 *PARK9*-mutant DA neurons at day 60, 90, 120 after the initiation of differentiation (n = 3, *p =
763 0.0052, **p = 0.0001, ***p = 0.0002).
764 (**F**) Immunoblot analysis of α-syn proteins in four control, two *PARK9*-mutant and *SNCA*
765 triplication DA neurons at Day 60 after the initiation of differentiation. After normalization to
766 β-iii-tubulin, the relative α-syn levels are shown as fold changes compared with control 1 (T-x
767 soluble, n = 3, p = 0.0603, Cont1 vs Triplication, SDS soluble, n = 3, p = 0.3726, Cont1 vs
768 Triplication). The statistical analysis was conducted using one-way ANOVA Tukey *post hoc* test.
769
770 **Fig. 2-1. iPSC-derived DA neurons on microfluidics**
771

JNeurosci Accepted Manuscript

772 (**A**) DA neurons analyzed by immunocytochemistry using FOXA2 (red) and tyrosine hydroxylase
773 (TH) (green) at day 60.
774 (**B**) DA neurons analyzed by immunocytochemistry using LMX1a (red) and tyrosine hydroxylase
775 (TH) (green) at day 60.
776 (**C**) DA neurons analyzed by immunocytochemistry using β-iii-tubulin (β-iii-tub) (red) and
777 tyrosine hydroxylase (TH) (green) at day 60 after the initiation of differentiation.
778 (**D**) After incubation with α-syn 555 for 15 min, DA neurons were fixed and treated with 0.2%
779 trypan blue to quench extracellular α-syn 555. Representative images of control (left) and
780 *PARK9*-mutated DA neurons (right) in orthogonal projections of confocal z-stacks. Arrows show
781 internalized α-syn 555.
782 (**E**) The time course of α-syn 555 internalization in control and *PARK9*-mutated DA neurons.
783 Scale bars represent 100 μm for Figure **A to C**. White scale bars represent 50 μm and black
784 scale bars represent 7.6 μm for Cont 3 and 13.6 μm for Mut2 in Figure **D**.
785
786 **Fig. 3-1. Modulation of *PARK9* expression levels**
787
788 (**A**) Real time PCR analysis of human ATP13A2 expressions in Cont1, Cont2, Mut1, Mut2 and
789 Mut1 and Mut2 transfected with lentivirus carrying human ATP13A2 in fibroblasts (n = 3, **p* =
790 0.03, one-way ANOVA Tukey *post hoc* test).
791 (**B**) Real time PCR analysis of human ATP13A2 expressions in Cont1, Cont2, Mut1, Mut2 and
792 Mut1 and Mut2 transfected with lentivirus carrying human ATP13A2 in fibroblasts (n = 3, **p* =
793 0.031, ***p* = 0.0001, one-way ANOVA Tukey *post hoc* test).
794 (**C**) Real time PCR analysis of human ATP13A2 expressions in Scrb shRNA, shRNA against human
795 ATP13A2, empty plasmid (Mock) or plasmid containing human ATP13A2 in H4 cells (n = 3, **p* =
796 0.0429, ***p* = 0.0202, Student *t* test).
797
798 **Fig. 5-1. The effect of TRPML1 agonists on lysosomal exocytosis**
799
800 (**A**) The activity of GCase in the media from Cont1 fibroblasts with treatments of different dose
801 of three TRPML1 agonists, ML-SA1, SF-22 and MK6-83 (n = 3, **p* = 0.03, Student *t* test).
802 (**B**) The activity of GCase in DA neurons that were treated with three TRPML1 agonists, ML-SA1,
803 SF-22 and MK6-83 (n = 3, **p* = 0.03, one-way ANOVA Tukey *post hoc* test).
804 (**C**) At 72 hours after transfecting Scrb shRNA or each five different shRNA against human
805 TRPML1 in H4 cells, immunoblotting was conducted to quantify TRPML1 protein levels. (Upper)
806 The representative blotting image. (Bottom) Densiometric analysis of each blots (n = 3, **p* =
807 0.0001, Student *t* test).
808 (**D**) Fluorescence of Rhod dextran and Cascade blue was measured before and after 1 μM MK6-
809 83 treatment at 72 hours after transfecting either Scrb shRNA or shRNA against TRPML1 (Left
810 four columns), or at one hour after 10 mM adenosine or 100 uM $LaCl_3$ treatment (Right four
811 columns) (n = 3, **p* = 0.03, Student *t* test).
812 (**E, F**) (Left four columns) The effect of inhibition of TRPML1 on Baf1-mediated lysosomal
813 exocytosis. (**E**) At 72 hours after transfecting either Scrb shRNA or shRNA against TRPML1,
814 fluorescence of Rhod dextran and Cascade blue in Cont 1 fibroblast was measured before and
815 at one hour after 200nM Baf1 treatment (n = 3, **p* = 0.03, Student *t* test). (Right six columns)

JNeurosci Accepted Manuscript

816 At one hour after 10 mM adenosine or 100 uM $LaCl_3$ treatment, fluorescence of Rhod dextran
817 and Cascade blue was measured before and at one hour after treatment of 200nM Baf1
818 treatment (n = 3, *p = 0.03, Student *t* test). (**F**) The same experiments were conducted using
819 Mut 2 fibroblasts.
820 (**G**) The activity of GCase released in the media by 1 μM MK6-83 treatment from Cont 1 (left
821 four columns) and Mut 1 fibroblasts (right four columns) was measured after pretreatment(s)
822 of lenti-virus mediated PARK9 overexpression and/or BAPTA-mediated lysosomal Ca^{2+} depletion
823 (n = 3, *p = 0.0322, **p = 0.0345, ***p = 0.0004, $^{\#}p$ = 0.0440, $^{\#\#}p$ = 0.0174, $^{\#\#\#}p$ = 0.0001 , one-
824 way ANOVA Tukey *post hoc* test).
825
826

JNeurosci Accepted Manuscript

827 **References:**

828 Bae M, Patel N, Xu H, Lee M, Tominaga-Yamanaka K, Nath A, Geiger J, Gorospe M, Mattson MP,
829 Haughey NJ (2014) Activation of TRPML1 clears intraneuronal Abeta in preclinical models of HIV
830 infection. J Neurosci 34:11485-11503.
831 Bento CF, Ashkenazi A, Jimenez-Sanchez M, Rubinsztein DC (2016) The Parkinson's disease-
832 associated genes ATP13A2 and SYT11 regulate autophagy via a common pathway. Nat Commun
833 7:11803.
834 Bliederhaeuser C, Grozdanov V, Speidel A, Zondler L, Ruf WP, Bayer H, Kiechle M, Feiler MS,
835 Freischmidt A, Brenner D, Witting A, Hengerer B, Fandrich M, Ludolph AC, Weishaupt JH,
836 Gillardon F, Danzer KM (2016) Age-dependent defects of alpha-synuclein oligomer uptake in
837 microglia and monocytes. Acta Neuropathol 131:379-391.
838 Borghi R, Marchese R, Negro A, Marinelli L, Forloni G, Zaccheo D, Abbruzzese G, Tabaton M
839 (2000) Full length alpha-synuclein is present in cerebrospinal fluid from Parkinson's disease and
840 normal subjects. Neurosci Lett 287:65-67.
841 Brahic M, Bousset L, Bieri G, Melki R, Gitler AD (2016) Axonal transport and secretion of fibrillar
842 forms of alpha-synuclein, Abeta42 peptide and HTTExon 1. Acta Neuropathol 131:539-548.
843 Burre J, Sharma M, Tsetsenis T, Buchman V, Etherton MR, Sudhof TC (2010) Alpha-synuclein
844 promotes SNARE-complex assembly in vivo and in vitro. Science 329:1663-1667.
845 Chartier-Harlin MC, Kachergus J, Roumier C, Mouroux V, Douay X, Lincoln S, Levecque C, Larvor
846 L, Andrieux J, Hulihan M, Waucquier N, Defebvre L, Amouyel P, Farrer M, Destee A (2004)
847 Alpha-synuclein locus duplication as a cause of familial Parkinson's disease. Lancet 364:1167-
848 1169.
849 Chen CC, Keller M, Hess M, Schiffmann R, Urban N, Wolfgardt A, Schaefer M, Bracher F, Biel M,
850 Wahl-Schott C, Grimm C (2014) A small molecule restores function to TRPML1 mutant isoforms
851 responsible for mucolipidosis type IV. Nat Commun 5:4681.
852 Cooper O et al. (2012) Pharmacological rescue of mitochondrial deficits in iPSC-derived neural
853 cells from patients with familial Parkinson's disease. Sci Transl Med 4:141ra190.
854 Dehay B, Ramirez A, Martinez-Vicente M, Perier C, Canron MH, Doudnikoff E, Vital A, Vila M,
855 Klein C, Bezard E (2012) Loss of P-type ATPase ATP13A2/PARK9 function induces general
856 lysosomal deficiency and leads to Parkinson disease neurodegeneration. Proc Natl Acad Sci U S
857 A 109:9611-9616.
858 Demirsoy S, Martin S, Motamedi S, van Veen S, Holemans T, Van den Haute C, Jordanova A,
859 Baekelandt V, Vangheluwe P, Agostinis P (2017) ATP13A2/PARK9 regulates endo-/lysosomal
860 cargo sorting and proteostasis through a novel PI(3, 5)P2-mediated scaffolding function. Hum
861 Mol Genet 26:1656-1669.
862 Dong XP, Wang X, Shen D, Chen S, Liu M, Wang Y, Mills E, Cheng X, Delling M, Xu H (2009)
863 Activating mutations of the TRPML1 channel revealed by proline-scanning mutagenesis. J Biol
864 Chem 284:32040-32052.
865 Dryanovski DI, Guzman JN, Xie Z, Galteri DJ, Volpicelli-Daley LA, Lee VM, Miller RJ, Schumacker
866 PT, Surmeier DJ (2013) Calcium entry and alpha-synuclein inclusions elevate dendritic
867 mitochondrial oxidant stress in dopaminergic neurons. J Neurosci 33:10154-10164.

JNeurosci Accepted Manuscript

868 Eisele YS, Monteiro C, Fearns C, Encalada SE, Wiseman RL, Powers ET, Kelly JW (2015) Targeting
869 protein aggregation for the treatment of degenerative diseases. Nat Rev Drug Discov 14:759-
870 780.
871 Gitler AD, Chesi A, Geddie ML, Strathearn KE, Hamamichi S, Hill KJ, Caldwell KA, Caldwell GA,
872 Cooper AA, Rochet JC, Lindquist S (2009) Alpha-synuclein is part of a diverse and highly
873 conserved interaction network that includes PARK9 and manganese toxicity. Nat Genet 41:308-
874 315.
875 Grunewald A, Arns B, Seibler P, Rakovic A, Munchau A, Ramirez A, Sue CM, Klein C (2012)
876 ATP13A2 mutations impair mitochondrial function in fibroblasts from patients with Kufor-Rakeb
877 syndrome. Neurobiol Aging 33:1843 e1841-1847.
878 Holemans T, Sorensen DM, van Veen S, Martin S, Hermans D, Kemmer GC, Van den Haute C,
879 Baekelandt V, Gunther Pomorski T, Agostinis P, Wuytack F, Palmgren M, Eggermont J,
880 Vangheluwe P (2015) A lipid switch unlocks Parkinson's disease-associated ATP13A2. Proc Natl
881 Acad Sci U S A 112:9040-9045.
882 Ibanez P, Bonnet AM, Debarges B, Lohmann E, Tison F, Pollak P, Agid Y, Durr A, Brice A (2004)
883 Causal relation between alpha-synuclein gene duplication and familial Parkinson's disease.
884 Lancet 364:1169-1171.
885 Kaushik S, Cuervo AM (2009) Methods to monitor chaperone-mediated autophagy. Methods
886 Enzymol 452:297-324.
887 Kong SM, Chan BK, Park JS, Hill KJ, Aitken JB, Cottle L, Farghaian H, Cole AR, Lay PA, Sue CM,
888 Cooper AA (2014) Parkinson's disease-linked human PARK9/ATP13A2 maintains zinc
889 homeostasis and promotes alpha-Synuclein externalization via exosomes. Hum Mol Genet
890 23:2816-2833.
891 Kriks S, Shim JW, Piao J, Ganat YM, Wakeman DR, Xie Z, Carrillo-Reid L, Auyeung G, Antonacci C,
892 Buch A, Yang L, Beal MF, Surmeier DJ, Kordower JH, Tabar V, Studer L (2011) Dopamine neurons
893 derived from human ES cells efficiently engraft in animal models of Parkinson's disease. Nature
894 480:547-551.
895 Lang AE, Lozano AM (1998) Parkinson's disease. First of two parts. N Engl J Med 339:1044-1053.
896 Lloyd-Evans E, Morgan AJ, He X, Smith DA, Elliot-Smith E, Sillence DJ, Churchill GC, Schuchman
897 EH, Galione A, Platt FM (2008) Niemann-Pick disease type C1 is a sphingosine storage disease
898 that causes deregulation of lysosomal calcium. Nat Med 14:1247-1255.
899 Lopes da Fonseca T, Pinho R, Outeiro TF (2016) A familial ATP13A2 mutation enhances alpha-
900 synuclein aggregation and promotes cell death. Hum Mol Genet 25:2959-2971.
901 Mazzulli JR, Zunke F, Isacson O, Studer L, Krainc D (2016a) alpha-Synuclein-induced lysosomal
902 dysfunction occurs through disruptions in protein trafficking in human midbrain
903 synucleinopathy models. Proc Natl Acad Sci U S A 113:1931-1936.
904 Mazzulli JR, Xu YH, Sun Y, Knight AL, McLean PJ, Caldwell GA, Sidransky E, Grabowski GA, Krainc
905 D (2011) Gaucher disease glucocerebrosidase and alpha-synuclein form a bidirectional
906 pathogenic loop in synucleinopathies. Cell 146:37-52.
907 Mazzulli JR, Zunke F, Tsunemi T, Toker NJ, Jeon S, Burbulla LF, Patnaik S, Sidransky E, Marugan
908 JJ, Sue CM, Krainc D (2016b) Activation of beta-Glucocerebrosidase Reduces Pathological alpha-
909 Synuclein and Restores Lysosomal Function in Parkinson's Patient Midbrain Neurons. J Neurosci
910 36:7693-7706.

JNeurosci Accepted Manuscript

911 Mc Donald JM, Krainc D (2017) Lysosomal Proteins as a Therapeutic Target in
912 Neurodegeneration. Annu Rev Med 68:445-458.
913 Medina DL, Fraldi A, Bouche V, Annunziata F, Mansueto G, Spampanato C, Puri C, Pignata A,
914 Martina JA, Sardiello M, Palmieri M, Polishchuk R, Puertollano R, Ballabio A (2011)
915 Transcriptional activation of lysosomal exocytosis promotes cellular clearance. Dev Cell 21:421-
916 430.
917 Morgan AJ, Davis LC, Galione A (2015) Imaging approaches to measuring lysosomal calcium.
918 Methods Cell Biol 126:159-195.
919 Park JS, Koentjoro B, Veivers D, Mackay-Sim A, Sue CM (2014) Parkinson's disease-associated
920 human ATP13A2 (PARK9) deficiency causes zinc dyshomeostasis and mitochondrial dysfunction.
921 Hum Mol Genet 23:2802-2815.
922 Raffaello A, Mammucari C, Gherardi G, Rizzuto R (2016) Calcium at the Center of Cell Signaling:
923 Interplay between Endoplasmic Reticulum, Mitochondria, and Lysosomes. Trends Biochem Sci
924 41:1035-1049.
925 Ramirez A, Heimbach A, Grundemann J, Stiller B, Hampshire D, Cid LP, Goebel I, Mubaidin AF,
926 Wriekat AL, Roeper J, Al-Din A, Hillmer AM, Karsak M, Liss B, Woods CG, Behrens MI, Kubisch C
927 (2006) Hereditary parkinsonism with dementia is caused by mutations in ATP13A2, encoding a
928 lysosomal type 5 P-type ATPase. Nat Genet 38:1184-1191.
929 Reddy A, Caler EV, Andrews NW (2001) Plasma membrane repair is mediated by Ca(2+)-
930 regulated exocytosis of lysosomes. Cell 106:157-169.
931 Rubinsztein DC (2006) The roles of intracellular protein-degradation pathways in
932 neurodegeneration. Nature 443:780-786.
933 Samie M et al. (2013) A TRP channel in the lysosome regulates large particle phagocytosis via
934 focal exocytosis. Dev Cell 26:511-524.
935 Samie MA, Xu H (2014) Lysosomal exocytosis and lipid storage disorders. J Lipid Res 55:995-
936 1009.
937 Shen D, Wang X, Li X, Zhang X, Yao Z, Dibble S, Dong XP, Yu T, Lieberman AP, Showalter HD, Xu
938 H (2012) Lipid storage disorders block lysosomal trafficking by inhibiting a TRP channel and
939 lysosomal calcium release. Nat Commun 3:731.
940 Singleton AB et al. (2003) alpha-Synuclein locus triplication causes Parkinson's disease. Science
941 302:841.
942 Surmeier DJ, Obeso JA, Halliday GM (2017) Selective neuronal vulnerability in Parkinson
943 disease. Nat Rev Neurosci 18:101-113.
944 Tardieux I, Webster P, Ravesloot J, Boron W, Lunn JA, Heuser JE, Andrews NW (1992) Lysosome
945 recruitment and fusion are early events required for trypanosome invasion of mammalian cells.
946 Cell 71:1117-1130.
947 Tarradas A, Selga E, Beltran-Alvarez P, Perez-Serra A, Riuro H, Pico F, Iglesias A, Campuzano O,
948 Castro-Urda V, Fernandez-Lozano I, Perez GJ, Scornik FS, Brugada R (2013) A novel missense
949 mutation, I890T, in the pore region of cardiac sodium channel causes Brugada syndrome. PLoS
950 One 8:e53220.
951 Tsunemi T, Krainc D (2014) Zn(2)(+) dyshomeostasis caused by loss of ATP13A2/PARK9 leads to
952 lysosomal dysfunction and alpha-synuclein accumulation. Hum Mol Genet 23:2791-2801.
953 Tsunemi T, Hamada K, Krainc D (2014) ATP13A2/PARK9 regulates secretion of exosomes and
954 alpha-synuclein. J Neurosci 34:15281-15287.

JNeurosci Accepted Manuscript

955 Usenovic M, Tresse E, Mazzulli JR, Taylor JP, Krainc D (2012) Deficiency of ATP13A2 leads to
956 lysosomal dysfunction, alpha-synuclein accumulation, and neurotoxicity. J Neurosci 32:4240-
957 4246.
958 Wong YC, Krainc D (2017) alpha-synuclein toxicity in neurodegeneration: mechanism and
959 therapeutic strategies. Nat Med 23:1-13.
960 Xu H, Ren D (2015) Lysosomal physiology. Annu Rev Physiol 77:57-80.
961 Zhong XZ, Zou Y, Sun X, Dong G, Cao Q, Pandey A, Rainey JK, Zhu X, Dong XP (2017) Inhibition of
962 Transient Receptor Potential Channel Mucolipin-1 (TRPML1) by Lysosomal Adenosine Involved
963 in Severe Combined Immunodeficiency Diseases. J Biol Chem 292:3445-3455.

964

JNeurosci Accepted Manuscript

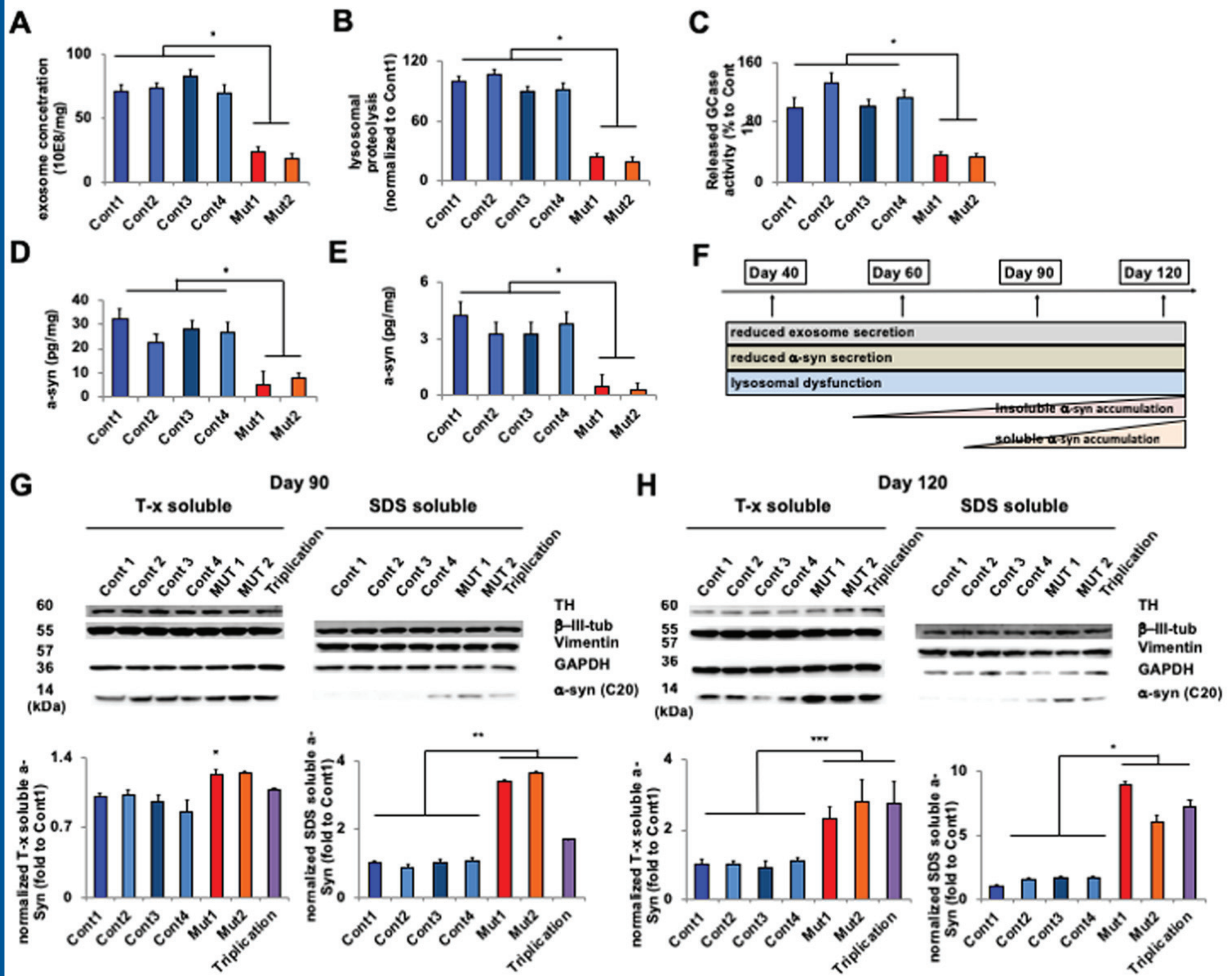

JNeurosci Accepted Manuscript

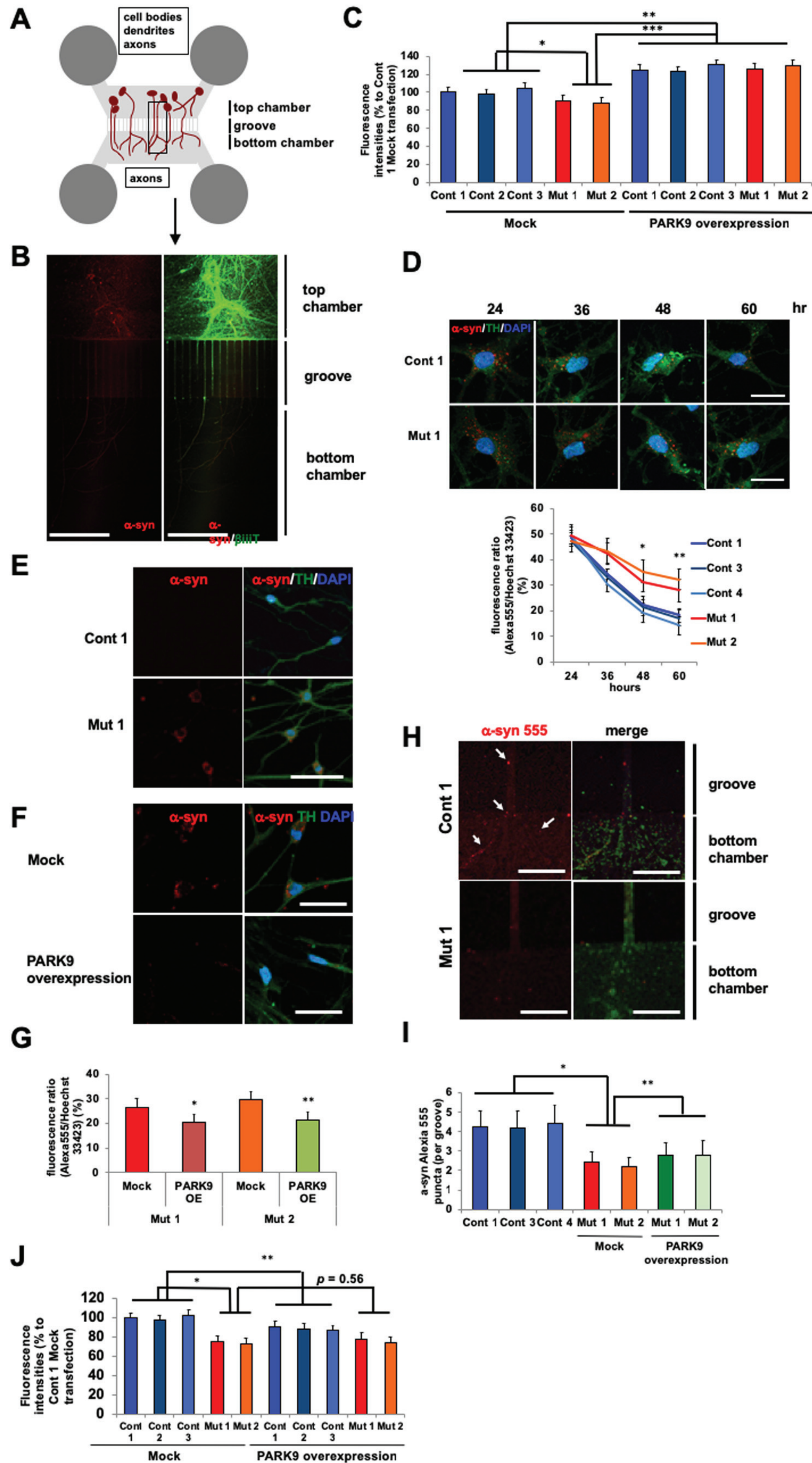

JNeurosci Accepted Manuscript

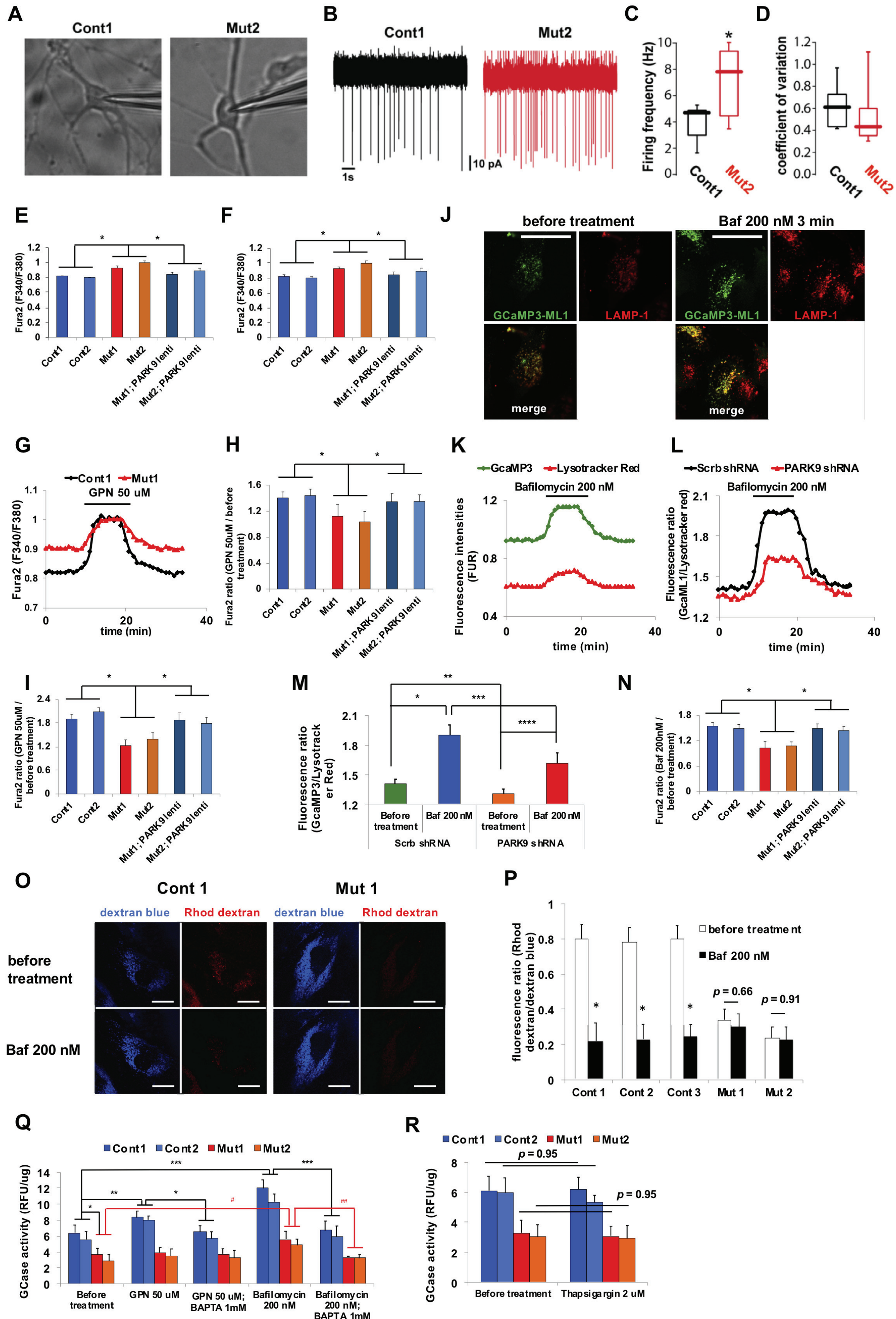

JNeurosci Accepted Manuscript

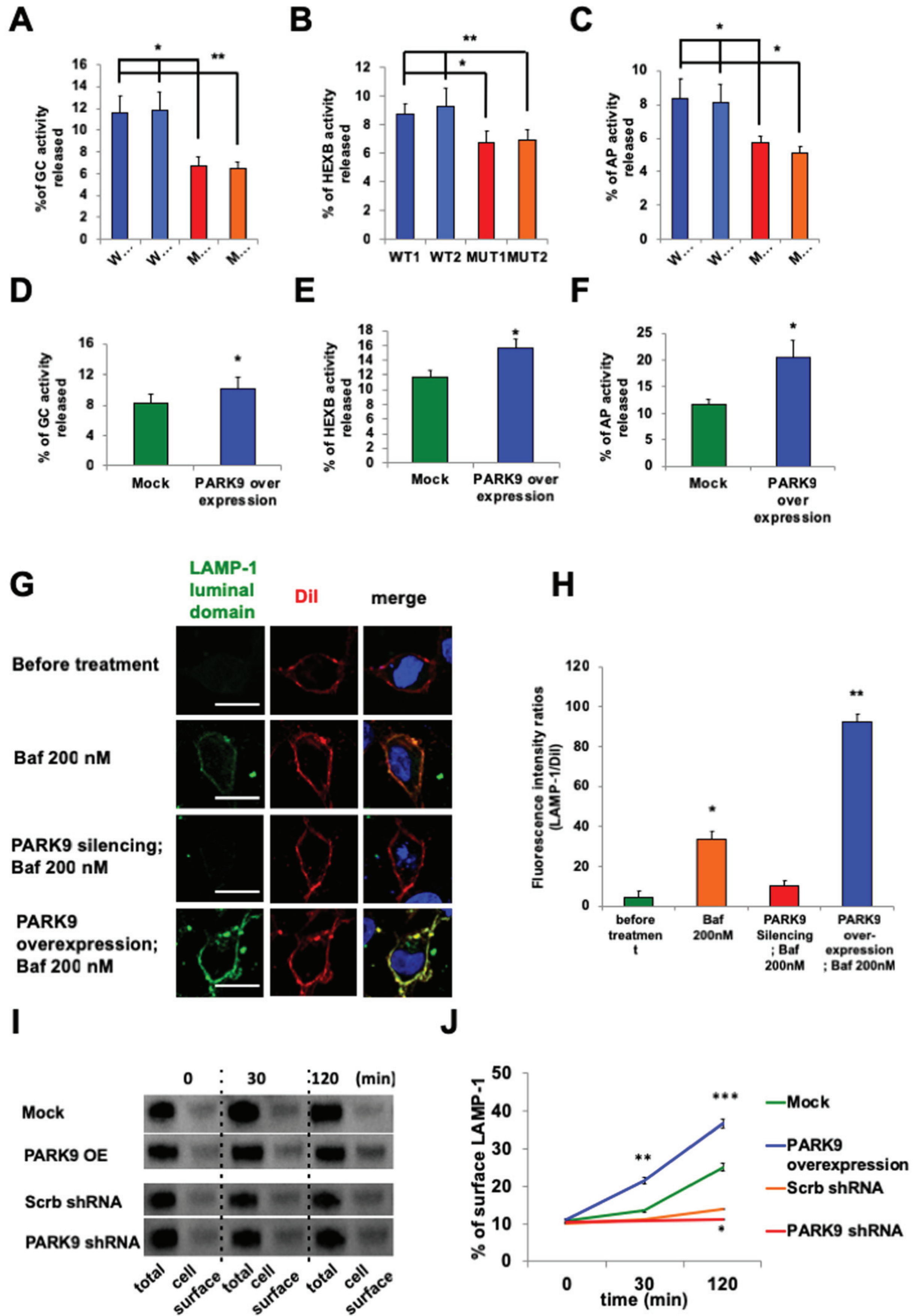

JNeurosci Accepted Manuscript